Interferometric Imaging Using Shared Quantum Entanglement

Matthew R. Brown[ORCID],[1] Markus Allgaier,[1] Valérian Thiel,[2] John D. Monnier[ORCID],[3] Michael G. Raymer[ORCID],[1] and Brian J. Smith[1,*]

[1]*Department of Physics and Oregon Center for Optical, Molecular, and Quantum Science, University of Oregon, Eugene, Oregon 97403, USA*
[2]*PASQAL, 7 rue Léonard de Vinci, 91300 Massy, France*
[3]*Department of Astronomy, University of Michigan, Ann Arbor, Michigan 48109, USA*

Quantum entanglement-based imaging promises significantly increased resolution by extending the spatial separation of optical collection apertures used in very-long-baseline interferometry for astronomy and geodesy. We report a tabletop entanglement-based interferometric imaging technique that utilizes two entangled field modes serving as a phase reference between two apertures. The spatial distribution of a simulated thermal light source is determined by interfering light collected at each aperture with one of the entangled fields and performing joint measurements. This experiment demonstrates the ability of entanglement to implement interferometric imaging.

Coherent measurement of light entering separate collection apertures of an imaging system, an approach called aperture synthesis that forms the basis of interferometric imaging, enables increased angular resolution beyond the single-aperture diffraction limit, as first demonstrated by Michelson and Pease [1]. The resolution of interferometric imaging is limited, in principle, only by the aperture separation (the "baseline"). Unlike interferometric imaging in the radio frequency (rf) band, where Earth-sized telescope arrays have been implemented based on locally recording the rf fields at each telescope [2], in the optical band (visible and near-infrared) the maximum baseline length is limited, in part, by the difficulty in performing local coherent detection with low noise at the few-photon level. The desire to increase angular resolution in the optical band by increasing the baseline is motivated by a number of applications currently limited by resolution: the search for exoplanets and the study of their atmospheres, resolved imaging of black hole event horizons in the near-infrared to complement the mm-wave imaging of the Event Horizon Telescope, geodesy, imaging of planet-forming disks, and stellar surfaces beyond the Sun [3–8]. This has prompted the quantum information science community to search for new tools such as shared optical entanglement between the receivers to extend optical interferometric imaging baselines [9–17].

There are three common approaches to achieving high angular resolution with synthetic apertures: (1) transporting the received fields to a central location and interfering them (direct interference) as depicted in Fig. 1(a); (2) distributing and interfering strong, mutually coherent fields—known as local oscillators (LOs)—with two received fields as shown in Fig. 1(b); or (3) measuring intensity correlations between
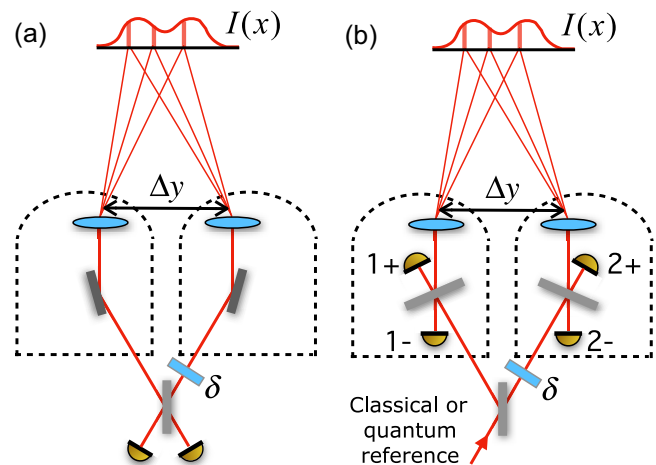

FIG. 1. Schematics of two approaches to interferometric imaging. Light from a distant incoherent source with intensity distribution $I(x)$ is collected by apertures with baseline Δy. (a) Direct interference combines the collected fields at a beam splitter with a known variable phase shift, δ, and performs intensity measurements at the output. (b) Indirect interference combines the collected fields with reference fields (laser light or path-entangled single-photon state) followed by local measurements at each aperture. Correlations between measurement outcomes at each telescope yield the mutual coherence function of the fields collected by the two telescope stations.

the collected fields as in the Hanbury Brown–Twiss experiment [18–21]. In the first approach, the challenge to increasing the baseline lies in constructing low-loss optical channels between telescopes, with the current state-of-the-art baseline being 330 m long [22]. The second approach is limited by the photon-number uncertainty of the LO (also called shot noise) as noted by Townes [23]. In the optical regime, direct interference is typically preferred due to its higher signal-to-noise ratio compared to interference with a classical LO [24,25]. In contrast, rf interferometric imaging (e.g., the Event Horizon Telescope) uses LOs since the effect of shot noise is significantly reduced: for the same average energy as one photon in the optical field, the rf field contains approximately 10^6 photons [23]. The third (Hanbury Brown–Twiss) approach is limited to relatively bright sources since it requires detection of at least two photons from the astronomical source, whereas the other methods require only one photon.

In this Letter, we present an experimental realization of an interferometric imaging technique that utilizes quantum entanglement as proposed by Gottesman, Jennewein, and Croke (GJC) [9]. To increase the baseline while delivering high signal-to-noise ratio at optical wavelengths, GJC proposed the use of a distributed, path-entangled single-photon state as a shared phase reference in conjunction with a quantum repeater network to alleviate transmission losses [9]. A path-entangled reference state (PERS) can be generated by, e.g., splitting a single photon occupying a single traveling mode into two paths of (un)equal length using a beam splitter (BS) [26–28]. The entangled state of the two modes (1 and 2) in the Fock basis is

$$|\psi_{\text{PERS}}\rangle = \frac{1}{\sqrt{2}}(|1\rangle_1|0\rangle_2 + e^{i\delta}|0\rangle_1|1\rangle_2). \qquad (1)$$

In the present application, the state provides a phase reference, δ, between two locations while minimizing the shot noise associated with the reference field.

The two paths are interfered with light collected by the apertures, as depicted in Fig. 1(b). A coincidence detection event between photon-counting detectors at each aperture, labeled ± 1 and ± 2 in Fig. 1(b), realizes a quantum joint measurement allowing coherent detection. For weak pseudothermal sources, schemes using joint quantum measurements of the received fields (e.g., direct interference or the GJC protocol) can yield more information per received photon than any scheme using independent measurements at each receiver (e.g., using classical LOs) [10]. Here, independent measurements are defined generally to include local operations and classical communication.

Interferometric imaging is based on measurement of the complex degree of coherence of an electromagnetic field after propagation from a source [29]. In the detection plane, the complex degree of coherence is given by $j(\vec{y}_1, \vec{y}_2) = \langle E^*(\vec{y}_1)E(\vec{y}_2)\rangle / \sqrt{\langle|E(\vec{y}_1)|^2\rangle\langle|E(\vec{y}_2)|^2\rangle}$, where

the electric field, E, is evaluated at two points labeled by transverse position vectors, $\vec{y}_1$ and $\vec{y}_2$, and angle brackets imply ensemble averaging. The complex visibility, $v(\Delta\vec{y})e^{i\phi(\Delta\vec{y})}$, arising from the interference of the fields collected at $\vec{y}_1$ and $\vec{y}_2$ is equal to $j(\vec{y}_1, \vec{y}_2)$. The van Cittert–Zernike theorem for a spatially incoherent source parallel to the detection plane shows that $v(\Delta\vec{y})e^{i\phi(\Delta\vec{y})}$ is proportional to the Fourier transform of the normalized source intensity distribution—$I(\vec{x}) = \langle|E(\vec{x})|^2\rangle / \iint\langle|E(\vec{x})|^2\rangle d^2x$, where $\vec{x}$ is the transverse position vector in the source plane—and depends on the displacement, $\Delta\vec{y} = \vec{y}_2 - \vec{y}_1$, between $\vec{y}_1$ and $\vec{y}_2$, and the difference of their distance from the optical axis, $r = |\vec{y}_2|^2 - |\vec{y}_1|^2$:

$$v(\Delta\vec{y})e^{i\phi(\Delta\vec{y})} = e^{\frac{-i\pi r}{\lambda z}} \iint I(\vec{x})e^{\frac{-i2\pi\vec{x}\cdot\Delta\vec{y}}{\lambda z}}d^2x. \qquad (2)$$

Here, z is the distance from the source plane to the observation plane and λ is the wavelength [30–33]. In interferometric imaging, measuring the complex visibility enables reconstruction of the source intensity distribution.

Our experimental setup demonstrating the GJC scheme is shown in Fig. 2. It consists of a pulsed heralded single-photon source and a pseudothermal light source in a single spectral-temporal mode mimicking filtered light from a star, which enables mode matching of the two sources. Both sources are derived from a titanium-sapphire (Ti:Sa) laser with 80 MHz repetition rate, 830 nm central wavelength and approximately 10 nm FWHM bandwidth. To simulate starlight, i.e., a spatially incoherent light source, we direct a 5 mW laser beam onto a double-slit mask placed 5 mm in front of a rotating, nearly Lambertian diffuser. The scattered light propagates 1.02 m to the detection plane resulting in a transverse coherence area on the order of a few square millimeters. A balanced, free-space BS separates the field into two spatial paths, enabling simultaneous coupling into two bare, polarization-maintaining, single-mode fibers (Thorlabs PM780-HP) with a core diameter of 5 μm, acting as small-aperture telescopes. One of the fibers, T1, is scanned in transverse position (y_1), to sample the field over a range of 6 mm in 10 μm steps. The other fiber, T2, is statically positioned in the center of the scattered field. Scattered light from the rotating diffuser creates a time-varying speckle pattern in the far field so that a single spatial mode exhibits thermal (Bose-Einstein) photon-number statistics [defined as $p(n) = \bar{n}^n/(\bar{n}+1)^{n+1}$] with average photon number $\bar{n} \approx 0.008$ and second-order coherence $g^{(2)}(0) = 2.00 \pm 0.05$ [34]. Because the intensity distribution in the far field is spread over a region greater than 10 cm, each fiber collects the same mean photon number, $\bar{n}$, as long as the fibers are not displaced more than a few millimeters from one another. The joint state of the collected fields is described by a density matrix, ρ_{ij}^{kl}; with i and k labeling powers of creation and annihilation operators for the field at T1, and j and l
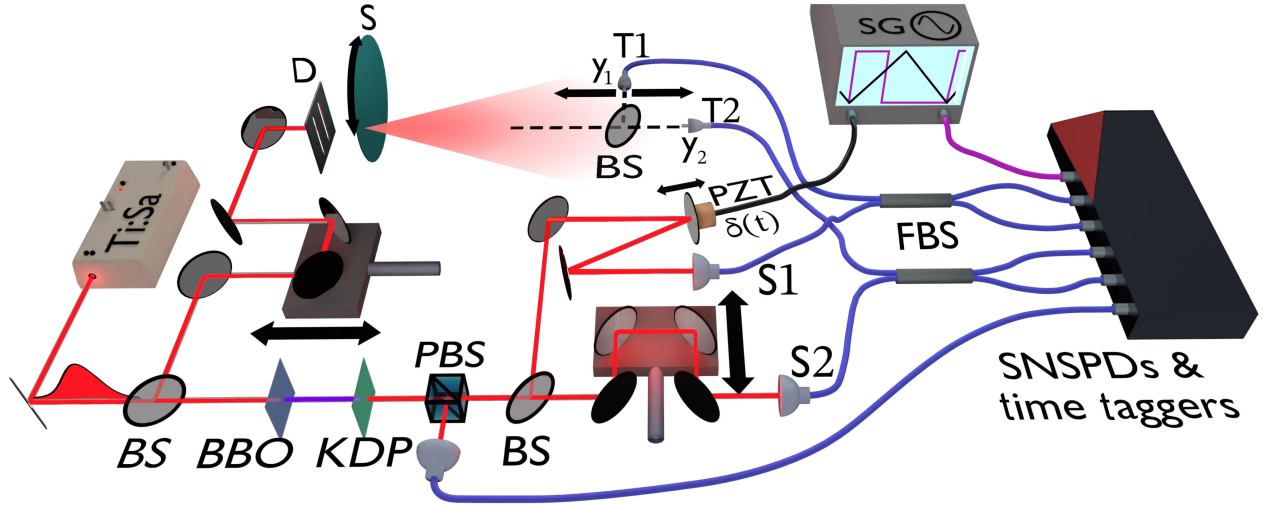
FIG. 2. A titanium-sapphire (Ti:Sa) laser is separated into two paths by a beam splitter (BS). One path creates a single spectral-temporal-mode thermallike state by passing through a double slit (D) and then a time-varying scatterer (S). The scattered light is collected by fibers T1 and T2 after a BS. The other path undergoes second-harmonic generation in a BBO crystal followed by parametric down conversion in a KDP crystal. The generated photon pair is split at a polarizing BS (PBS); one output is used for heralding. The heralded photon is sent to a BS to generate the path-entangled reference state along two paths, with one path having a time-dependent length controlled by a PZT to introduce a phase shift, $\delta(t)$, driven by a signal generator (SG). Each path is coupled into single-mode fibers (S1 and S2), and combined with the fields collected by T1 and T2 in two fiber BSs (FBSs). The outputs of the FBSs are monitored by superconducting nanowire single-photon detectors (SNSPDs) and time taggers.

playing similar roles at T2. Further details throughout the Letter are given in the Supplemental Material [35].

The main beam from the Ti:Sa (1.24 W) is frequency-doubled to a wavelength of 415 nm in a 700 μm-thick beta barium borate (BBO) crystal to produce a 100 mW beam that pumps an 8 mm-thick potassium dihydrogen phosphate (KDP) crystal phase-matched for degenerate, collinear, type-II spontaneous parametric down-conversion (SPDC), which is designed to produce photons in the same spectral-temporal mode as the pseudothermal source. The source produces a two-mode squeezed-vacuum state that is nearly spectrally separable with a central wavelength of 830 nm where the herald mode, vertically polarized (V), has ~5 nm of bandwidth FWHM, while the heralded mode, horizontally polarized (H), has a bandwidth of ~12 nm FWHM [45]. A polarizing BS separates the H and V fields, where the V field is sent to a single-mode fiber connected to a superconducting nanowire single-photon detector (SNSPD). We measure an unheralded second-order coherence $g^{(2)}(0) = 1.66 \pm 0.06$ (which implies a Schmidt number of 1.51 and near separability [46]) and an average photon number of approximately 0.01, after correcting for detection efficiency. A detection event at the heralding detector indicates the presence of a single photon (or more) in the heralded field. The density operator of the heralded field in the photon-number basis is approximately $\rho_{\text{heralded}} \approx \eta p(1)|1\rangle\langle 1| + (2-\eta)\eta p(2)|2\rangle\langle 2|$, where $\eta \approx 0.28$ is the measured heralding efficiency and $p(n)$ are thermal photon-number probabilities, indicating the possibility of more than one photon in the pulse.

The heralded field is directed to a 50:50 BS realizing the PERS in Eq. (1). A mirror bonded to a piezoelectric translator (PZT) in one path introduces a controllable, relative phase difference between the two paths. The PZT is controlled by a signal generator (SG) that applies a 600 Hz triangular waveform, giving a time-dependent phase, $\delta(t)$, which varies between 0 and approximately 4π. The heralded PERS distributed to the telescopes is approximately given by Eq. (1), which neglects the vacuum and higher-order photon numbers (a proof that the full state is entangled is given in the Supplemental Material [35]). The two paths are coupled into polarization-maintaining, single-mode fibers, indicated by S1 and S2 in Fig. 2.

The complex visibility of the simulated starlight, as defined in Eq. (2), is measured by interfering the two modes of the PERS, S1 and S2, with the fields collected by the two fibers acting as telescopes, T1 and T2 in Fig. 2, at fiber BSs (FBSs). The FBS outputs are sent to SNSPDs. All detection events are time-tagged using a time-to-digital converter. We keep coincidence events only when they are registered between different telescopes. The coincidence events, occurring probabilistically at times t_j, can be associated with a known PZT phase, $\delta(t_j)$, by comparison to a phase-locked square voltage pulse used as a clock indicating the change in direction of the PZT. The set of event phases are used to estimate the complex visibility (see Supplemental Material [35] and [47] for details).

Theory predicts the estimated visibility measured by our experiment to be (see Supplemental Material [35])
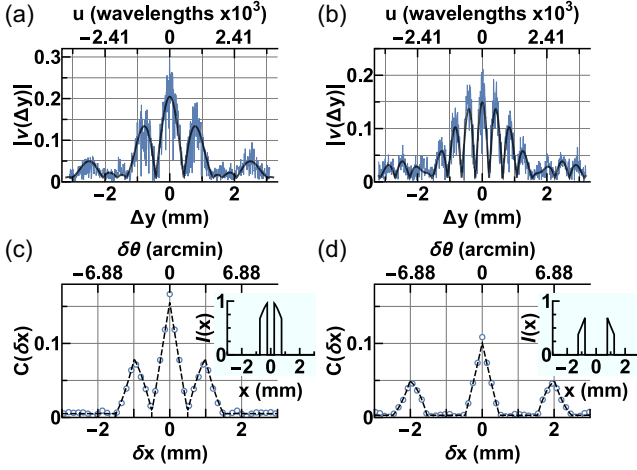
FIG. 3. (a), (b) show the measured magnitude of the complex visibility, $|\tilde{v}(\Delta y)|$, versus telescope separation, Δy, in mm and, u, the number of wavelengths for double slits with 1 and 2 mm separation, respectively. The points are linearly interpolated to guide the eye. The black line is a model fit that takes parameters found from the fits shown in (c), (d) and adjusts scaling and offset. (c), (d) show the reconstructed autocorrelation of the source distribution for the 1 and 2 mm slit separations versus position in mm and arcmin. Experimental error bars are subsumed by the circular points used (see Supplemental Material [35] for details). The dashed black lines are the best model fits. Insets show the unnormalized source intensity distributions estimated from the model fit parameters.

$$\tilde{v}(\Delta \vec{y})e^{i\tilde{\phi}(\Delta \vec{y})} \approx \pm \frac{2p(1)\mathrm{Re}[\rho_{10}^{01}e^{i\delta}]\Gamma}{(2-\eta)p(2)\rho_{00}^{00} + p(1)(\rho_{10}^{10} + \rho_{01}^{01})}, \quad (3)$$

where $\pm$ is the phase difference acquired from the FBSs determined by which detectors register events, ρ is the density matrix of the collected star photons that depends on Eq. (2), $p(n)$ is the Bose distribution of the two-mode squeezed state from the SPDC, η is the heralding efficiency, $\Gamma \approx 0.5$ denotes the coherent overlap of the idler field mode from the SPDC and the field collected from the pseudo-thermal source. Given the experimental parameters, the predicted maximum value of $|\tilde{v}|$ from Eq. (3) is 0.24.

In this experiment, the magnitude of the complex visibility versus baseline is measured. The relative phase of the interferometer paths fluctuates on a 10 s timescale, which is typically longer than necessary to acquire sufficient coincidence events to determine the amplitude and phase of the complex visibility at a given baseline, but does not allow a stationary phase reference between the measurements at different separations. However, the Fourier transform of the phase-independent, modulus-squared complex visibility as a function of baseline, $|v(\Delta \vec{y})|^2$, yields the autocorrelation of the normalized source intensity distribution, $C(\delta x) = \int I(x)I(x+\delta x)dx$ (see Supplemental Material [35]). Such a reconstruction without

TABLE I. Autocorrelation fit parameters (σ, d, and w) for the double slits with 0.5 mm slit width, and slit separations of 1 mm ($d = 0.5$ mm) and 2 mm ($d = 1$ mm), which are illuminated by the same Gaussian beam.

	1 mm slits	2 mm slits
σ(mm)	1.678 ± 0.271	1.784 ± 0.142
d(mm)	0.494 ± 0.005	1.006 ± 0.004
w(mm)	0.508 ± 0.006	0.476 ± 0.006

interferometer stability is sufficient to verify a source distribution using a model fit.

For two known source distributions created from 0.5 mm wide vertically oriented double slits separated by 1 or 2 mm, illuminated by a Gaussian-profile beam, Figs. 3(a) and 3(b) show the magnitude of the complex visibility as a function of baseline in the horizontal direction, $\Delta \vec{y}$. Each data point in the measured visibility results from processing around 10 000 collected events—the PZT phases at the time of a coincidence, $\delta(t_j)$—over 10 s (see Supplemental Material [35] and [47]). The Fourier transform of the squared visibility is proportional to the autocorrelation of the source intensity distribution, shown in Figs. 3(c) and 3(d). The estimated errors, which are equal in size to the circular points, account for statistical errors and phase fluctuations, but do not account for systematic errors. We also show a best fit of the reconstructed autocorrelation data to a model based on the autocorrelation of an intensity distribution describing the experiment (see Supplemental Material [35]). Parameters in the model are the distance from the center of a slit to the midpoint between the slits, d; the width of the slits, w; and the radius of the common Gaussian beam illuminating the slits, σ.

The best-fit parameters and errors determined using maximum likelihood estimation for the sources are shown in Table I and found to lie within fabrication tolerances of the slits (± 20 μm). We also find that, as expected, the fitted Gaussian beam radius parameter in the two cases are equal within error. Overall, the fit to the expected intensity distributions for the two slits indicates that the GJC scheme is capable of source reconstruction.

In conclusion, we have shown that an approximately single-photon state distributed across two paths can act as an entangled-state phase and amplitude reference for use in distributed very-long-baseline interferometry, as proposed by GJC [9]. The complex degree of coherence of a distant incoherent source was determined and served to reconstruct its intensity distribution. To achieve extended baselines, future work will study true thermal sources, reduce higher-order photon-number contributions, and extend the scheme to detection of multiple spectral-temporal modes with the purpose of increasing detection rates. Lengthening baselines will require a quantum repeater chain to distribute the path-entangled light with lower loss than using optical fiber

alone [48,49]. Correcting for turbulence-induced phase distortion by the Earth's atmosphere is possible in arrays with three or more telescopes using closure phase [50], and progress toward such an implementation with PERSs can be found in [15]. Further, it was proposed that a quantum network in which single-photon states could be stored in quantum memories and used on demand could provide a further increase in multiplexing ability [11,12,16,17]. While functioning quantum networks are years in the future, if successful the proposed scheme could become one of the first practical uses of a quantum network and would open new horizons in visible-wavelength astronomical imaging.

---

*Corresponding author: bjsmith@uoregon.edu

[1] A. A. Michelson and F. G. Pease, Measurement of the diameter of Alpha-Orionis by the interferometer, Proc. Natl. Acad. Sci. U.S.A. **7**, 143 (1921).

[2] R. C. Walker, Very long baseline interferometry, in *Synthesis Imaging in Radio Astronomy II*, edited by G. B. Taylor, C. L. Carilli, and R. A. Perley, ASP Conference Series Vol. 180 (Astronomical Society of the Pacific, San Fransisco, California, 1999), Chap. 22, pp. 433–462.

[3] K. Akiyama *et al.* (Event Horizon Telescope Collaboration), First M87 event horizon telescope results. I. The shadow of the supermassive black hole, Astrophys. J. Lett. **875**, L1 (2019).

[4] K. Akiyama *et al.* (Event Horizon Telescope Collaboration), First M87 event horizon telescope results. II. Array and instrumentation, Astrophys. J. Lett. **875**, L2 (2019).

[5] K. Akiyama *et al.* (Event Horizon Telescope Collaboration), First sagittarius A* event horizon telescope results. I. The shadow of the supermassive black hole in the center of the milky way, Astrophys. J. Lett. **930**, L12 (2022).

[6] H. Schuh and D. Behrend, Vlbi: A fascinating technique for geodesy and astrometry, J. Geodyn. **61**, 68 (2012).

[7] N. Ibrahim, J. D. Monnier, S. Kraus, J.-B. Le Bouquin, N. Anugu, F. Baron, T. ten Brummelaar, C. L. Davies, J. Ennis, T. Gardner, A. Labdon, C. Lanthermann, A. Mérand, E. Rich, G. H. Schaefer, and B. R. Setterholm, Imaging the inner astronomical unit of the Herbig Be star HD 190073, Astrophys. J. **947**, 68 (2023).

[8] J. D. Monnier, M. Zhao, E. Pedretti, N. Thureau, M. Ireland, P. Muirhead, J.-P. Berger, R. Millan-Gabet, G. Van Belle, T. ten Brummelaar, H. McAlister, S. Ridgway, N. Turner, L. Sturmann, J. Sturmann, and D. Berger, Imaging the surface of Altair, Science **317**, 342 (2007).

[9] D. Gottesman, T. Jennewein, and S. Croke, Longer-baseline telescopes using quantum repeaters, Phys. Rev. Lett. **109**, 070503 (2012).

[10] M. Tsang, Quantum nonlocality in weak-thermal-light interferometry, Phys. Rev. Lett. **107**, 270402 (2011).

[11] E. T. Khabiboulline, J. Borregaard, K. De Greve, and M. D. Lukin, Quantum-assisted telescope arrays, Phys. Rev. A **100**, 022316 (2019).

[12] E. T. Khabiboulline, J. Borregaard, K. De Greve, and M. D. Lukin, Optical interferometry with quantum networks, Phys. Rev. Lett. **123**, 070504 (2019).

[13] L. A. Howard, G. G. Gillett, M. E. Pearce, R. A. Abrahao, T. J. Weinhold, P. Kok, and A. G. White, Optimal imaging of remote bodies using quantum detectors, Phys. Rev. Lett. **123**, 143604 (2019).

[14] M. M. Marchese and P. Kok, Large baseline optical imaging assisted by single photons and linear quantum optics, Phys. Rev. Lett. **130**, 160801 (2023).

[15] D. Diaz, Y. Zhang, V. O. Lorenz, and P. G. Kwiat, Emulating quantum-enhanced long-baseline interferometric telescopy, in *Frontiers in Optics + Laser Science* (Optical Society of America, Washington, 2021), pp. FTh6D–7.

[16] R. Czupryniak, J. Steinmetz, P. G. Kwiat, and A. N. Jordan, Optimal photonic gates for quantum-enhanced telescopes, arXiv:2108.01170.

[17] R. Czupryniak, E. Chitambar, J. Steinmetz, and A. N. Jordan, Quantum telescopy clock games, Phys. Rev. A **106**, 032424 (2022).

[18] R. Hanbury Brown, R. C. Jennison, and M. K. Das Gupta, Apparent angular sizes of discrete radio sources: Observations at Jodrell Bank, Manchester, Nature (London) **170**, 1061 (1952).

[19] R. Hanbury Brown and R. Q. Twiss, Correlation between photons in two coherent beams of light, Nature (London) **177**, 27 (1956).

[20] R. Hanbury Brown and R. Q. Twiss, 2. A test of a new type of stellar interferometer on sirius, in *A Source Book in Astronomy and Astrophysics, 1900–1975* (Harvard University Press, Cambridge, MA, 2013), pp. 8–12.

[21] P. Stankus, A. Nomerotski, A. Slosar, and S. Vintskevich, Two-photon amplitude interferometry for precision astrometry, Open J. Astrophys. **5** (2022). 10.21105/astro.2010 .09100

[22] T. A. ten Brummelaar, H. A. McAlister, S. T. Ridgway, W. G. Bagnuolo Jr., N. H. Turner, L. Sturmann, J. Sturmann, D. H. Berger, C. E. Ogden, R. Cadman, W. I. Hartkopf, C. H. Hopper, and M. A. Shure, First results from the CHARA array. II. A description of the instrument, Astrophys. J. **628**, 453 (2005).

[23] C. H. Townes, Noise and sensitivity in interferometry, in *Principles of Long Baseline Stellar Interferometry*, edited by Peter Lawson (JPL, Pasadena, California, 2000) Chap. 4, pp. 59–70.

[24] D. D. S. Hale, M. Bester, W. C. Danchi, W. Fitelson, S. Hoss, E. A. Lipman, J. D. Monnier, P. G. Tuthill, and C. H. Townes, The Berkeley infrared spatial interferometer: A heterodyne stellar interferometer for the mid-infrared, Astrophys. J. **537**, 998 (2000).

[25] M. J. Ireland and J. D. Monnier, A dispersed heterodyne design for the planet formation imager, in *Optical and*

Infrared Interferometry IV, Society of Photo-Optical Instrumentation Engineers (SPIE) Conference Series edited by J. K. Rajagopal, M. J. Creech-Eakman, and F. Malbet (SPIE, Bellingham, Washington, 2014), Vol. 9146, p. 914612.

[26] B. J. Oliver and C. R. Stroud Jr, Predictions of violations of Bell's inequality in an 8-port homodyne detector, Phys. Lett. A **135**, 407 (1989).

[27] S. M. Tan, D. F. Walls, and M. J. Collett, Nonlocality of a single photon, Phys. Rev. Lett. **66**, 252 (1991).

[28] S. J. van Enk, Single-particle entanglement, Phys. Rev. A **72**, 064306 (2005).

[29] L. Mandel and E. Wolf, *Optical Coherence and Quantum Optics* (Cambridge University Press, Cambridge, England, 1995).

[30] M. Born and E. Wolf, *Principles of Optics: Electromagnetic Theory of Propagation, Interference and Diffraction of Light* (Elsevier, New York, 2013).

[31] P. H. van Cittert, Die wahrscheinliche Schwingungsverteilung in einer von einer Lichtquelle direkt oder mittels einer Linse beleuchteten Ebene, Physica **1**, 201 (1934).

[32] F. Zernike, The concept of degree of coherence and its application to optical problems, Physica (Amsterdam) **5**, 785 (1938).

[33] J. W. Goodman, *Statistical Optics* (John Wiley & Sons, New York, 2015).

[34] L. E. Estes, L. M. Narducci, and R. A. Tuft, Scattering of light from a rotating ground glass, J. Opt. Soc. Am. **61**, 1301 (1971).

[35] See Supplemental Material at http://link.aps.org/supplemental/10.1103/PhysRevLett.131.210801 for derivation of (4), more exposition on materials and methods, and an explanation of error analysis and model fitting, which includes Refs. [36–44].

[36] D. B. Horoshko, S. De Bièvre, G. Patera, and M. I. Kolobov, Thermal-difference states of light: Quantum states of heralded photons, Phys. Rev. A **100**, 053831 (2019).

[37] J. Sperling and W. Vogel, Verifying continuous-variable entanglement in finite spaces, Phys. Rev. A **79**, 052313 (2009).

[38] A. Peres, Separability criterion for density matrices, Phys. Rev. Lett. **77**, 1413 (1996).

[39] M. Horodecki, P. Horodecki, and R. Horodecki, Separability of mixed states: Necessary and sufficient conditions, Phys. Lett. A **223**, 1 (1996).

[40] B. Saleh, *Photoelectron Statistics: With Applications to Spectroscopy and Optical Communication* (Springer, New York, 2013), Vol. 6.

[41] I. A. Walmsley and M. G. Raymer, Experimental study of the macroscopic quantum fluctuations of partially coherent stimulated Raman scattering, Phys. Rev. A **33**, 382 (1986).

[42] Z.-Y. J. Ou, *Multi-Photon Quantum Interference* (Springer, New York, 2007), Vol. 43.

[43] D. F. Williams, C.-M. Wang, and U. Arz, In-phase/quadrature covariance-matrix representation of the uncertainty of vectors and complex numbers, in *2006 68th ARFTG Conference: Microwave Measurement* (IEEE, New York, 2006), pp. 1–4.

[44] J. Hurt, Asymptotic expansions of functions of statistics, Aplikace matematiky **21**, 444 (1976).

[45] P. J. Mosley, J. S. Lundeen, B. J. Smith, P. Wasylczyk, A. B. U'Ren, C. Silberhorn, and I. A. Walmsley, Heralded generation of ultrafast single photons in pure quantum states, Phys. Rev. Lett. **100**, 133601 (2008).

[46] A. Christ, K. Laiho, A. Eckstein, K. N. Cassemiro, and C. Silberhorn, Probing multimode squeezing with correlation functions, New J. Phys. **13**, 033027 (2011).

[47] A. Tamimi, T. Landes, J. Lavoie, M. G. Raymer, and A. H. Marcus, Fluorescence-detected Fourier transform electronic spectroscopy by phase-tagged photon counting, Opt. Express **28**, 25194 (2020).

[48] L.-M. Duan, M. D. Lukin, J. I. Cirac, and P. Zoller, Long-distance quantum communication with atomic ensembles and linear optics, Nature (London) **414**, 413 (2001).

[49] N. Sangouard, C. Simon, J. Minář, H. Zbinden, H. de Riedmatten, and N. Gisin, Long-distance entanglement distribution with single-photon sources, Phys. Rev. A **76**, 050301(R) (2007).

[50] J. D. Monnier, Optical interferometry in astronomy, Rep. Prog. Phys. **66**, 789 (2003).